

Spatial Degradation-Aware and Temporal Consistent Diffusion Model for Compressed Video Super-Resolution

Hongyu An^{1,2}, Xinfeng Zhang^{1*}, Shijie Zhao² and Li Zhang²

¹School of Computer Science and Technology, University of Chinese Academy of Sciences

²Bytedance Inc.

anhongyu22@mails.ucas.ac.cn, xfzhang@ucas.ac.cn, {zhaoshijie.0526, lizhang.idm}@bytedance.com

Abstract

Due to limitations of storage and bandwidth, videos stored and transmitted on the Internet are usually low-quality with low-resolution and compression noise. Although video super-resolution (VSR) is an efficient technique to enhance video resolution, relatively VSR methods focus on compressed videos. Directly applying general VSR approaches leads to the failure of improving practical videos, especially when frames are highly compressed at a low bit rate. Recently, diffusion models have achieved superior performance in low-level visual tasks, and their high-realism generation capability enables them to be applied in VSR. To synthesize more compression-lost details and refine temporal consistency, we propose a novel Spatial Degradation-Aware and Temporal Consistent (SDATC) diffusion model for compressed VSR. Specifically, we introduce a distortion Control module (DCM) to modulate diffusion model inputs and guide the generation. Next, the diffusion model executes the denoising process for texture generation with fine-tuned spatial prompt-based compression-aware module (PCAM) and spatio-temporal attention module (STAM). PCAM extracts features to encode specific compression information dynamically. STAM extends the spatial attention mechanism to a spatio-temporal dimension for capturing temporal correlation. Extensive experimental results on benchmark datasets demonstrate the effectiveness of the proposed modules in enhancing compressed videos.

1 Introduction

Limited by the high costs of memory and transmission, videos are usually down-sampled and compressed in practical scenarios. Video super-resolution (VSR) is an efficient technique to improve video visual quality, which aims to recover continuous high-resolution (HR) frames from corresponding low-resolution (LR) frames. With the development

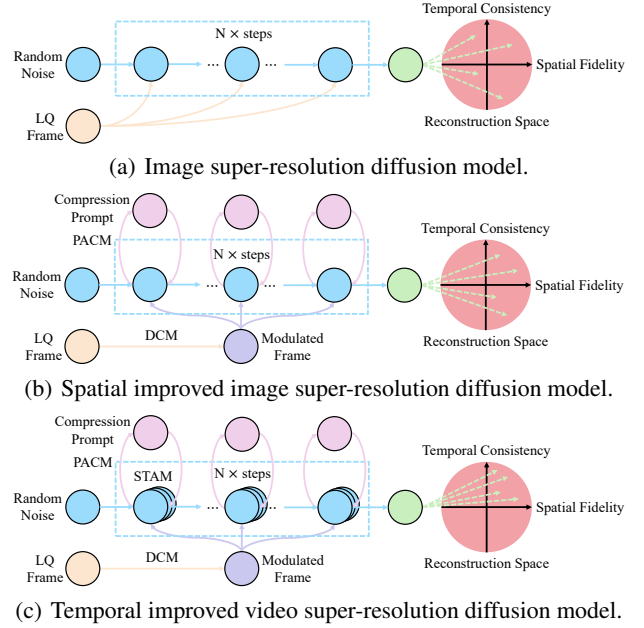


Figure 1: Comparison of different diffusion processes for image super-resolution. Compared with (a) StableSR, our SDATC introduces spatial (b) and temporal (c) guidance for better generation.

of deep learning, sliding windows network-based and recurrent network-based approaches have achieved great breakthroughs. Unfortunately, these methods hardly consider real-world videos stored and delivered on the Internet or mobile devices, which are always compressed with different levels [Wang *et al.*, 2023b]. Therefore, existing VSR methods may regard compression artifacts as textures and enlarge them during reconstruction. Meanwhile, compression non-adaptive VSR models lead to blurred restoration.

To address the above issues, several works have investigated VSR on compressed videos. COMISR [Li *et al.*, 2021] exploited compression properties to reduce distortions. FTVSR [Qiu *et al.*, 2022] proposed a frequency Transformer for compressed VSR. CAVSR [Wang *et al.*, 2023b] utilized video stream information and predicted the compression ratio. Although these approaches improved compressed VSR performance with additional encoding priors beyond compressed frames, restoring truncated textures is still challenging. The quantization process during compression inevitably

*Corresponding author.

introduces information loss, thus the lack of low-quality (LQ) video priors makes it difficult to reconstruct pleasant details.

Inspired by the vivid generation capability of diffusion models, we apply generation priors to solve the above challenges. Recently, some studies have handled the image super-resolution (SR) task with a diffusion model. SR3 [Saharia *et al.*, 2022] pioneeringly utilized denoising diffusion probabilistic models (DDPM) to achieve image SR. The innovative StableSR [Wang *et al.*, 2024] and DiffBIR [Lin *et al.*, 2025] leveraged ControlNet [Zhang *et al.*, 2023] to balance the realism and fidelity of reconstruction results. Following works [Sun *et al.*, 2023; Wu *et al.*, 2024; Sun *et al.*, 2024] employed content-related textual prompts as guidance. An intuitive way to realize SR for compressed videos is to recover each frame through the mentioned diffusion models. However, the stochastic diffusion process damages temporal consistency. Limited works [Yang *et al.*, 2025; Zhou *et al.*, 2024] explored the temporal alignment for diffusion-based VSR.

The gap between existing diffusion models and the compressed VSR task lies in two main aspects: (1) How to improve diffusion models to generate frames with higher spatial fidelity and fewer compression artifacts? (2) How to constrain the temporal consistency of reconstructed frames? To mitigate these gaps, we design a distortion control module (DCM) to modulate diffusion model inputs. DCM eliminates interfering noise in input frames and controls the following diffusion phase based on LQ priors to prevent mistaken artifact generation. Subsequently, we insert a prompt-based compression-aware module (PCAM) at UNet and VAE decoders to incorporate compression awareness. Based on compression feature code, PCAM provides lightweight prompts to characterize different degradation degree information. Finally, to constrain temporal consistency, we employ a spatio-temporal attention module (STAM), which explores relationships across frames with a spatial-temporal dimension fusion.

In general, the proposed Spatial Degradation-Aware and Temporal Consistent (SDATC) diffusion model relieves compression negative impacts during spatial generation as shown in Fig.1(b). In contrast to current SR diffusion models, we divide the compressed VSR task into two sub-tasks. DCM preemptively eases degradation effects and PACM guides diffusion with compression-aware prompts. As depicted in Fig.1(c), STAM further takes full advantage of adjacent frames to smooth reconstruction frames.

The main technique contributions of this work can be summarized as follows:

- We propose a distortion control module (DCM) to adjust diffusion input distribution and provide controllable guidance. The end-to-end DCM reduces content-independent degradations for the generation process.
- We introduce a prompt-based compression-aware module (PCAM) in UNet and VAE decoders to extract compression information from latent and reconstruction space. PCAM enables an adaptive diffusion process for frames compressed to varying degrees.
- We design a spatio-temporal attention module (STAM) and optical flow-based latent features warping to enhance temporal coherence.

2 Related Work

2.1 Video Super-Resolution

VSR exploits spatio-temporal similarity across LR videos to recover HR videos. VSRNet [Kappeler *et al.*, 2016] first employed a deep learning model for VSR. DUF [Jo *et al.*, 2018] applied 3D convolution to leverage spatio-temporal relationships dynamically. EDVR [Wang *et al.*, 2019] proposed Deformable Convolutional Networks (DCN) [Dai *et al.*, 2017] based feature alignment and fusion. TDAN [Tian *et al.*, 2020] further utilized DCN to estimate motion offsets between target, prior, and following frames. BasicVSR++ [Chan *et al.*, 2022a] designed a bidirectional recurrent architecture. VRT [Liang *et al.*, 2024] applied a Transformer-based recurrent framework. However, the simple Bicubic down-sampling simulation of these methods brings about synthetic-to-real gaps, which cause the failure of compressed VSR.

2.2 Compressed Video Super-Resolution

The complex compression degradation poses new challenges for compressed VSR. To explore compression priors, COMISR [Li *et al.*, 2021] dealt with the location and smoothness of compressed frames through enhancement modules. FTVSR [Qiu *et al.*, 2022] designed a DCT-based attention module to preserve high-frequency details. CAVSR [Wang *et al.*, 2023b] estimated the compression level and applied corresponding treatments. Several works [Yang *et al.*, 2021; Wang *et al.*, 2021; Chan *et al.*, 2022b] tackled real-world VSR by introducing more degradation types. The better compression estimation and more realistic degradation construction make efforts on compressed VSR, but the information loss is difficult to recover with limited priors, especially when frames are compressed at low bit rates.

2.3 Diffusion-based Video Super-Resolution

Diffusion-based image restoration has received growing attention from researchers recently. The great generation capability was explored in SISR [Saharia *et al.*, 2022]. StableSR [Wang *et al.*, 2024] and DiffBIR [Wang *et al.*, 2024] used the control module during reconstruction. CCSR [Sun *et al.*, 2023] improved content consistency through a structure refinement module. SUPIR [Yu *et al.*, 2024] modified the ControlNet and designed a novel connector ZeroSFT to reduce computational complexity, which enabled a large-scale image restoration model. SATeCo [Chen *et al.*, 2024] pivoted on learning spatial-temporal guidance from low-resolution videos. MGLD-VSR [Yang *et al.*, 2025] and Upscale-A-Video [Zhou *et al.*, 2024] tried to constrain the temporal consistency of diffusion-based VSR models. In this work, we leverage additional generation priors of pre-trained diffusion models to resolve the compressed VSR task. To handle the limitations of existing diffusion frameworks, we develop spatial degradation-aware and temporal consistent techniques. The degradation pre-processing and guidance could also become a paradigm for diffusion-based VSR models.

3 Methodology

Video compression (e.g., H.264 [Wiegand *et al.*, 2003]) inevitably introduces information loss which makes it diffi-

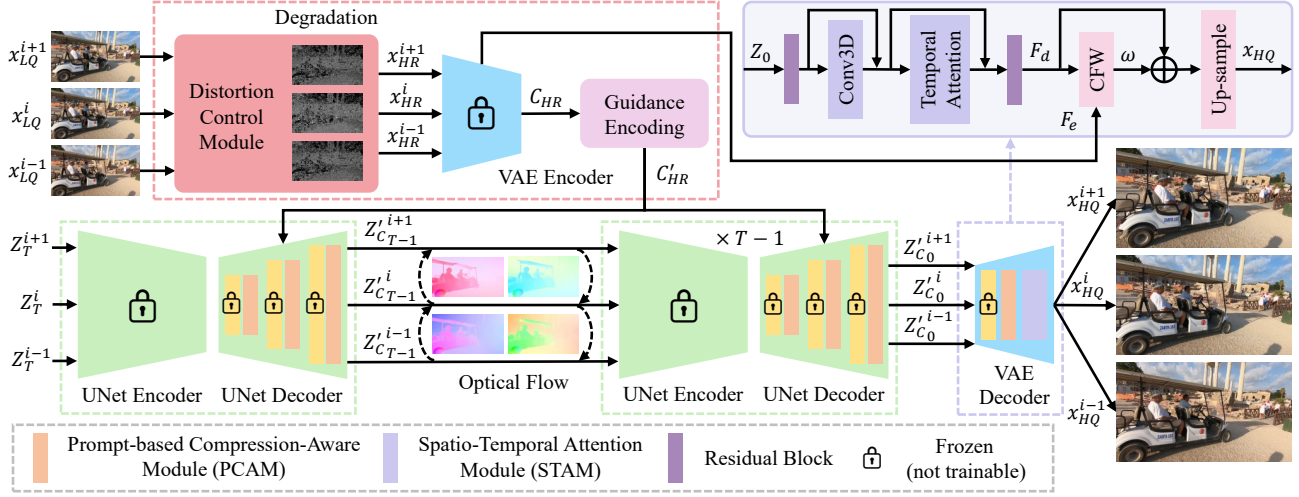


Figure 2: Overview of the proposed Spatial Degradation-Aware and Temporal Consistent (SDATC) diffusion network. We apply a distortion control module (DCM) to enhance input low-quality (LQ) frames and extract guidance. The modulated frames are fed into the Latent Diffusion Model (LDM) based framework. The trainable prompt-based compression-aware module (PCAM) catches degradation-specific details for generation. Moreover, we incorporate the fine-tuned spatio-temporal attention module (STAM) to preserve temporal consistency.

cult to reconstruct realistic details for compressed VSR. Motivated by the diffusion model success, we take advantage of generation priors in pre-trained Latent Diffusion Model (LDM) [Rombach *et al.*, 2022] for compressed VSR. Compared with diffusion models, LDM applies Variational Auto-Encoder (VAE) to map images into latent space for decreasing training costs, which enables large-scale dataset application with abundant prior knowledge. Nevertheless, the unstable LDM generation can not handle compressed videos at unknown levels and increases temporal inconsistency.

To tackle these challenges, we propose a Spatial Degradation-Aware and Temporal Consistent (SDATC) diffusion model with fewer unpleasant artifacts. The overall framework of SDATC is illustrated in Fig.2. We merely fine-tune UNet decoders in down-sampled latent space and VAE decoders in pixel-level reconstruction space. Such a framework with proposed modules prevents a great increase in computational complexity and improves spatio-temporal SR performance. Architecture details of the proposed modules are introduced in the following subsections.

3.1 Diffusion Model

Diffusion models generate images from random noise z through an iterative reverse Markovian. The data distribution learning for generation is through the T steps forward process. The diffusion from a clean image x_0 to Gaussian noise x_T can be formulated as:

$$x_t = \sqrt{\alpha_t}x_{t-1} + \sqrt{1 - \alpha_t}\epsilon_{t-1}, \quad (1)$$

$$x_t = \sqrt{\alpha_t}x_0 + \sqrt{1 - \alpha_t}\epsilon_t, \quad (2)$$

$$q(x_t|x_0) = N(x_t; \sqrt{\alpha_t}x_0, (1 - \alpha_t)I), \quad (3)$$

where $t \in [1, T]$, $\epsilon \in N(0, 1)$, and $\bar{\alpha}_t = \prod_{i=1}^t \alpha_i$. As t increases, α_i gradually decreases, when $T \rightarrow \infty$, $x_T \in N(0, 1)$. The reverse process predicts the inverse distribution based on the UNet network with the sampling process:

$$q(x_{t-1}|x_t, x_0) = N(x_{t-1}; \tilde{\mu}(x_t, x_0), \tilde{\beta}_t I). \quad (4)$$

The training goal is obtaining a denoising network ϵ_θ by minimizing $\mathbb{E}_{t \in [1, T], x_0, \epsilon_t} [\|\epsilon_t - \epsilon_\theta(x_t, t)\|^2]$ to estimate the noise ϵ_t . Based on the denoising network ϵ_θ , the model performs T iterations diffusion reverse denoising process.

3.2 Distortion Control Module

Given a n frames low-quality (LQ) video sequence $\{x_{LQ}^1, \dots, x_{LQ}^i, \dots, x_{LQ}^n\}$, we aim to recover a high quality (HQ) video sequence $\{x_{HQ}^1, \dots, x_{HQ}^i, \dots, x_{HQ}^n\}$. Most existing diffusion-based VSR methods first up-sample input frames to target resolution and then generate details through the diffusion process. Unfortunately, the widely utilized up-sample approaches Bilinear or Bicubic may destroy textures and have a negative influence on subsequent generations.

To address the above issues and concentrate on compression characteristics, we design a distortion control module (DCM). Notably, LDM learns input data distribution, thus original distortions in frames will interfere in the generation process with unpleasant artifacts. To prevent LDM from noise corruption, we execute DCM pre-processing and extract LQ guidance for the subsequent diffusion process. Specifically, we apply a Transformer-based network to remove distortions and increase spatial resolution as follows:

$$x_{HR} = \text{Up}(\text{RSTB}(\text{Conv}_{3 \times 3}(x_{LQ}))), \quad (5)$$

where $\text{RSTB}(\cdot)$ depicts Residual Swin Transformer Blocks [Liang *et al.*, 2021] and $\text{Up}(\cdot)$ is PixelShuffle up-sampling. Next, we encode modulated x_{HR} in condition latent space C_{HR} by VAE encoder. Following ControlNet [Zhang *et al.*, 2023], we input condition guidance C_{HR} concatenated with noise Z_t into a trainable copy of UNet encoder to encode guidance C'_{HR} . The UNet Decoder fine-tune training with guidance is then denoted as:

$$Z'_t = \text{UNet}_{\text{decoder}}(\text{Cat}(Z_t, \text{Conv}_{\text{zero}}(C'_{HR}))), \quad (6)$$

where $\text{Cat}(\cdot)$ stands for concatenation. Notably, we introduce zero convolution to prevent early-stage random noise fluctu-

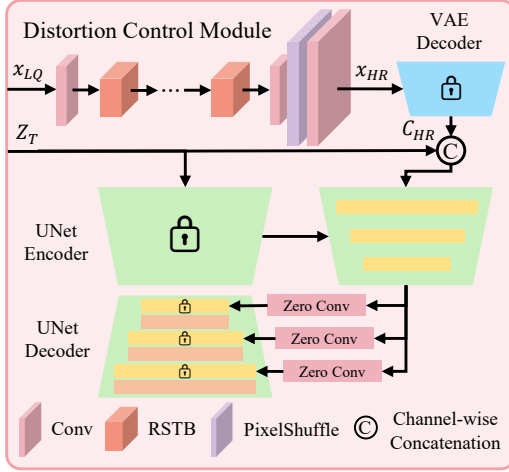


Figure 3: The distortion control module (DCM) designed as the pre-processing of the diffusion model.

ation. The proposed DCM is presented in Fig. 3, we design a general pre-processing module for diffusion-based VSR and encode modified conditions to guide generation. Moreover, we fine-tune DCM with LDM in an end-to-end framework to explore better generation input distribution and guidance.

3.3 Prompt-based Compression-Aware Module

Prompt learning has achieved great success in natural language processing with effective context information. Recently, PromptIR [Potlapalli *et al.*, 2024] developed prompt learning in image restoration. Inspired by PromptIR, we try to generate reasonable prompts for compression and diffusion generation. Nevertheless, the learnable weights of randomly initialized PromptIR prompts are obtained only by taking features average and simple linear mapping, which can not catch compression priors. Consequently, we leverage compression estimation to generate degradation dependence prompts. The proposed prompt-based compression-aware module (PCAM) is fine-tuned in both UNet and VAE decoders to guide in different spaces. Compared with large-scale degradation datasets pre-training or descriptions generated by complex semantic large language models, PCAM is feasible and has low computational complexity.

As depicted in Fig. 4, PCAM interacts with latent feature Z' via CNN and Adaptive AvgPool (AAP) to generate feature vector v , which encodes contextual and compression priors in prompt components P . We apply v to weight P and then upscale P to the specific Z' size as P_C because we develop PCAM in each scale of UNet and VAE decoders. The compression-aware prompts generation is summarized as:

$$P_C = \text{Conv}_{3 \times 3} \left(\sum_{k=1}^K \text{AAP}(\text{Conv}_{3 \times 3}(Z))_k P_k \right), \quad (7)$$

where k denotes prompt length. P_C enables interaction between latent feature Z' and prompt P to get compression information. Finally, we concatenate P_C with Z' and exploit compression-aware prompts through a Transformer block. The feature transformation can be formulated as:

$$Z'_C = \text{Conv}_{3 \times 3}(\text{Transformer}(\text{Cat}(Z, P_C))). \quad (8)$$

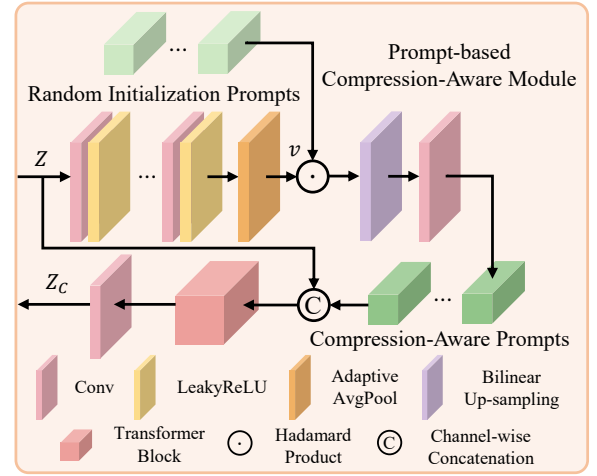


Figure 4: The prompt-based compression-aware module (PCAM). PCAM extracts compression degradation information as prompts to direct better details generation.

3.4 Spatio-Temporal Attention Module

Although LDM-based SR methods reconstruct each frame successfully, the multi-frame generation meets temporal inconsistency. The serious deformation of an object across adjacent frames is visually disastrous. To improve compressed VSR with temporal consistency, we introduce a spatio-temporal attention module (STAM) in the VAE decoder. In particular, we expand the temporal dimension with multi-frames. Freezing pre-trained spatial residual blocks, we insert 3D CNN and temporal attention block (TAB). TAB executes self-attention among temporal dimension and the outputs of TAB are regarded as residuals. We apply learnable parameters to balance spatio-temporal branches as:

$$Z'_0 = \text{Res}(\text{Conv}_{3 \times 3}(Z'_C)), \quad (9)$$

$$Z''_0 = \alpha_T \text{Conv}_{3 \times 3} \text{D}_{3 \times 3}(Z'_0) + (1 - \alpha_T)(Z'_0), \quad (10)$$

$$F_d = \text{Res}(\beta_T \text{TA}(Z''_0) + (1 - \beta_T)(Z''_0)), \quad (11)$$

where $\text{Res}(\cdot)$ is residual block, α_T and β_T denote learnable spatio-temporal tensors. As illustrated in Fig. 2, we further incorporate F_e from the VAE encoder and achieve a balanced outcome through Controllable Feature Warping (CFW) module [Wang *et al.*, 2024], the adjustable parameter ω controls reconstructed outputs as (a larger ω means higher fidelity):

$$x_{HQ} = \text{Up}(F_d + \omega \text{CFW}(F_e, F_d)). \quad (12)$$

Limited by computational complexity, we explore temporal coherence in the VAE decoder. In the latent space of UNet decoder, we compute forward and backward optical flow to align features for improving consistency. As shown in Fig. 2, we calculate the motion error E_t at each denoising step:

$$E_t = \sum_{i=1}^{N-1} \|f_b(Z'^i_t) - Z'^{i+1}_t\|_1 + \sum_{i=2}^N \|f_f(Z'^i_t) - Z'^{i-1}_t\|_1, \quad (13)$$

where f_b and f_f indicate backward and forward warping. The subsequent sampling process is as follows:

$$Z'_t = \text{UNet}(Z'_{t+1}) - \sigma_t^2 \nabla_Z(\text{UNet}(Z'_{t+1}), E_t). \quad (14)$$

Table 1: Quantitative comparison of $\times 4$ VSR on different compression level datasets. **Bold** and underlined values denote the best and second-best results respectively. \uparrow and \downarrow indicate better quality with higher and lower values correspondingly.

Dataset		REDS4					UDM10				
Method	CRF	DISTS \downarrow	FID \downarrow	NIQE \downarrow	MANIQA \uparrow	CLIP-IQA \uparrow	DISTS \downarrow	FID \downarrow	NIQE \downarrow	MANIQA \uparrow	CLIP-IQA \uparrow
BasicVSR++	15	0.1148	38.57	5.017	0.2338	0.4984	0.1028	39.63	5.914	0.2264	0.4539
VRT	15	0.1197	39.19	5.558	0.2406	0.5015	0.1055	39.15	6.487	0.2335	0.4635
FTVSR	15	0.0991	<u>33.68</u>	4.648	0.3385	0.6023	0.1005	37.24	6.070	0.3258	0.5463
Real-ESRGAN	15	0.0944	52.40	<u>2.631</u>	<u>0.4021</u>	0.5953	0.1023	52.67	4.354	0.3513	0.5577
RealBasicVSR	15	<u>0.0684</u>	36.08	2.647	0.3401	0.5295	0.1011	51.49	3.852	0.3400	0.4957
StableSR	15	0.0991	57.94	3.056	0.3733	0.7187	<u>0.0975</u>	51.62	4.361	0.3808	<u>0.6538</u>
MGLD-VSR	15	0.0732	34.78	2.887	0.3905	0.5417	0.1044	46.90	<u>3.810</u>	<u>0.3887</u>	0.5242
SDATC (Ours)	15	0.0636	31.09	2.613	0.4024	<u>0.6119</u>	0.0940	<u>38.52</u>	3.508	0.3935	0.6606
BasicVSR++	25	0.1861	94.19	6.019	0.1681	0.3637	0.1403	83.33	6.412	0.1947	0.3315
VRT	25	0.1902	93.75	6.496	0.1706	0.3766	0.1436	82.30	6.928	0.2016	0.3519
FTVSR	25	0.1649	84.59	5.697	0.2952	0.4611	0.1374	88.71	6.685	0.3015	0.4013
Real-ESRGAN	25	0.1191	73.99	2.871	0.3565	<u>0.5385</u>	0.1205	76.86	4.590	0.3139	0.4806
RealBasicVSR	25	0.1028	70.11	<u>2.839</u>	0.3267	0.5252	0.1272	80.02	3.860	0.3065	0.4445
StableSR	25	0.1292	74.60	3.440	0.3212	0.5370	<u>0.1155</u>	69.68	4.591	0.3498	<u>0.5960</u>
MGLD-VSR	25	<u>0.0975</u>	<u>55.37</u>	2.964	<u>0.3703</u>	0.5001	0.1191	67.00	<u>3.847</u>	<u>0.3628</u>	0.5003
SDATC (Ours)	25	0.0894	51.00	2.796	0.3796	0.5616	0.1153	66.15	3.524	0.3675	0.6021
BasicVSR++	35	0.2676	183.37	7.225	0.1037	0.2255	0.2173	163.68	7.267	0.1417	0.2055
VRT	35	0.2686	183.05	7.345	0.1049	0.2379	0.2198	163.22	7.656	0.1455	0.2159
FTVSR	35	0.2526	180.28	7.190	0.1983	0.1867	0.2106	162.23	7.730	0.2319	0.1706
Real-ESRGAN	35	0.2241	172.29	3.993	0.2329	0.4210	0.1937	155.43	5.489	0.2375	0.3138
RealBasicVSR	35	0.1720	137.54	3.158	0.2715	<u>0.4637</u>	0.1884	165.71	4.235	0.2649	0.3436
StableSR	35	0.2311	166.80	4.734	0.1576	0.2321	0.1868	149.57	5.630	0.2157	0.3378
MGLD-VSR	35	0.1587	97.90	<u>2.873</u>	<u>0.3275</u>	0.4598	0.1771	117.43	3.998	<u>0.2878</u>	<u>0.3808</u>
SDATC (Ours)	35	<u>0.1602</u>	<u>113.19</u>	2.725	0.3276	0.5545	0.1683	<u>146.33</u>	3.526	0.2958	0.4637

The first item is the DDPM result and the second is the optical flow warping gradient scaled by variance σ_t^2 . The gradient updating in UNet(Z'_{t+1}) is based on E_t .

4 Experiments

4.1 Implementation Details

Datasets

We train our SDATC on merged REDS [Nah *et al.*, 2019] training set and validation set, the left 4 sequences (REDS4) are for testing. During training, we utilize the x264 encoder to $\times 4$ down-sample and compress videos. Without loss of generality, we randomly compress videos from 10K to 100K bit rates. The x264 codec provides different compression levels, i.e., Constant Rate Factor (CRF). CRF value ranges from 0 to 51 and 0 stands for lossless compression. Following existing works [Li *et al.*, 2021; Qiu *et al.*, 2022; Wang *et al.*, 2023b], we choose CRFs of 15, 25, and 35 to generate compressed testing videos. We also conduct evaluations on the Vid4 dataset [Liu and Sun, 2013] and the UDM10 dataset [Yi *et al.*, 2019].

Training Setting

The DCM consists of 6 RSTB blocks with a window size of 8. We fine-tune the diffusion model on 8 NVIDIA A100 GPUs. The length of input clips is 5, the batch size is 4, and the patch size is 512. The learning rate is initialized as 5×10^{-5} using the Adam [Kingma, 2014] optimizer. The trade-off parameter ω is set to 0.75. During inference, we set 50 sampling steps.

Evaluation Setting

We apply perceptual metrics for evaluation, including DISTS [Ding *et al.*, 2020], FID [Heusel *et al.*, 2017], NIQE [Mit-

tal *et al.*, 2012], MANIQA [Yang *et al.*, 2022], and CLIP-IQA [Wang *et al.*, 2023a], which concentrate on human visual preference. Moreover, we comprehensively compare the proposed SDATC with VSR (BasicVSR++ [Chan *et al.*, 2022a], VRT [Liang *et al.*, 2024]), compressed VSR (Real-ESRGAN [Wang *et al.*, 2021], RealBasicVSR [Chan *et al.*, 2022b], FTVSR [Qiu *et al.*, 2022]), and diffusion-based models (StableSR [Wang *et al.*, 2024], MGLD-VSR [Yang *et al.*, 2025]).

4.2 Quantitative Comparison

The quantitative experimental results are shown in Tab. 1. It can be observed that our SDATC achieves the best performances on different compression levels in the REDS4 dataset and UDM10 dataset. The superior results demonstrate that adopting modules with compression-aware generation priors improves visual perception. Furthermore, the higher CLIP-IQA values of SDATC reflect its strong realistic details generation capability. We also present quantitative experiments on the Vid4 dataset in Appendix 1.2. The other metrics comparison like PSNR, SSIM, and LPIPS is also mentioned.

4.3 Qualitative Comparison

As can be seen from zoom-in regions of Fig. 5, the proposed SDATC outperforms MSE-based methods BasicVSR++, VRT, and FTVSR with clearer details, especially they rebuild completely blurry results when CRF=35. Compared with generative approaches, SDATC restores finer text and numbers in sequence “calendar”, more appealing textures in sequence “archpeople”, and more natural trees, grassland, and water surface in sequence “lake”. Note that the SOTA diffusion-based VSR method MGLD-VSR introduces grid-like artifacts in sequence archpeople and color shift artifacts



Figure 5: Qualitative comparison of $\times 4$ VSR on different compression level datasets.

SDATC (Ours)	71%	RealBasicVSR
SDATC (Ours)	76%	StableSR
SDATC (Ours)	60%	MGLD-VSR

Figure 6: User study results of $\times 4$ VSR on CRF=25 datasets.

in sequence lake. Alternatively, SDATC addresses such issues with compression-specific modules. More visual results on different datasets are provided in Appendix 1.2.

4.4 User Study

We further perform a user study to select the better videos from two reconstructed videos. In detail, we invite 15 participants to compare SDATC with RealBasicVSR, StableSR, and MGLD-VSR in pairs, respectively. The compared video sequences are set to 9. As depicted in Fig. 4, volunteers prefer the results of SDATC rather than other approaches.

Table 2: Ablation study of Distortion Control Module.

Module	DISTS↓	NIQE↓	MANIQA↑	CLIP-IQA↑
Baseline	0.1551	4.104	0.1694	0.1470
+USM	0.1451	4.107	0.1796	0.1670
+DiffBIR	0.1215	3.293	0.2655	0.3169
+TMSA	0.1408	3.475	0.2354	0.2486
+DCM	0.1005	2.964	0.3386	0.4371

5 Ablation Study

In this section, we further analyze the proposed SDATC diffusion network. In detail, we perform experiments on each module individually and observe their effectiveness in the spatio-temporal dimension. The experiments are conducted on the compressed REDS4 dataset (CRF=25) for $\times 4$ VSR.

5.1 Distortion Control Module

As depicted in Tab. 2, DCM improves perceptual quality and exceeds other enhancement methods. Specifically, Unsharpen Mask (USM) sharpens GT images to optimize train-

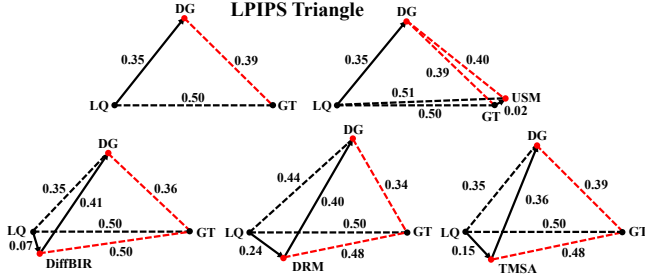


Figure 7: LPIPS scores of different restoration methods.

Table 3: Ablation study of Prompt-based Compression-Aware Module.

Module	PSNR \uparrow /SSIM \uparrow	NIQE \downarrow	MANIQA \uparrow	CLIP-IQA \uparrow
Baseline	26.26/0.7009	4.104	0.1694	0.1470
+Prompt	26.29/0.7006	3.882	0.1867	0.1767
+Softmax	26.32/0.7015	3.903	0.1861	0.1820
+PCAM	26.58/0.7110	3.803	0.2080	0.2053

Table 4: Ablation study of Prompt-based Compression-Aware Module Artifacts Removal.

Module	Perception-Sensitive Pixel Loss \downarrow		
	CRF=15	CRF=25	CRF=35
Baseline	0.2348	0.3137	0.5263
+PCAM	0.2058	0.2868	0.5072

ing. DiffBIR [Lin *et al.*, 2025] up-samples images by PixelShuffle and then restores them. TMSA [Liang *et al.*, 2024] extracts multi-frame features before up-sampling. In contrast to them, DCM achieves compression discrimination, activating higher fidelity generation results. To clarify intuitively, we calculate similarity scores of the low-quality (LQ) domain, diffusion generation (DG) domain, GT domain, and enhancement domain. The similarity is measured by LPIPS and FID, lower scores indicate closer distance. As presented in Fig. 6 (FID scores are in Appendix 1.2), basic diffusion-based VSR up-samples LQ frames by Bicubic and next executes diffusion denoising. Maintaining the generation capacity unchanged, DCM enables the diffusion model to generate results with better spatial fidelity. We also visualize the results of these methods in Appendix 1.2, DCM effectively deduces noises and provides smooth diffusion inputs.

5.2 Prompt-based Compression-Aware Module

It can be observed in Tab. 3 that PCAM achieves not only perceptual but also PSNR and SSIM gains over baseline. Note that “+Prompt” means the basic random initialization learnable-prompts. “+PCAM” is the proposed feature extraction and compression-aware prompts. “+Softmax” is the version of PCAM with a Softmax layer in feature extraction. PCAM provides compression-specific prompts to guide reasonable texture generation in the latent and reconstruction space. Simultaneously, the compression priors extracted from features contribute to pixel-oriented metrics. Furthermore, we perform an experiment on REDS4 dataset to quantitatively analyze compressed VSR artifacts. Following LDL [Liang *et al.*, 2022], we calculate perception-sensitive pixel loss based on variances. From Tab. 4, the PCAM module effectively distinguishes compression and generation artifacts.

Table 5: Ablation study of Spatio-Temporal Attention Module.

Module	VMAF \uparrow	NIQE \downarrow	MANIQA \uparrow	CLIP-IQA \uparrow
Baseline	35.70	4.104	0.1694	0.1470
+STAM	44.53	3.200	0.3620	0.4869
Real-ESRGAN	59.40	2.871	0.3565	0.5385
RealBasicVSR	64.66	2.839	0.3267	0.5252
StableSR	58.44	3.440	0.3212	0.5370
CCSR	51.99	2.920	0.3680	0.5355
MGLD-VSR	56.80	2.964	0.3703	0.5001
SDATC (Ours)	67.22	2.796	0.3796	0.5616

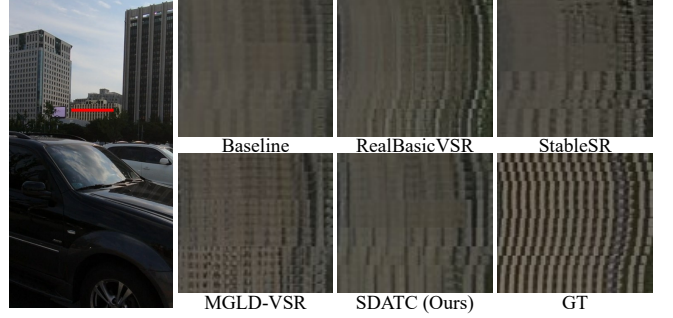


Figure 8: Temporal profiles comparison. The so-called temporal profiles are acquired through concatenating rows at the same location in continuous frames.

5.3 Spatio-Temporal Attention Module

To evaluate both spatial quality as well as temporal coherency, we adopt video quality assessment VMAF [Blog, 2016]. VMAF additionally introduces motion measures for temporal characteristics. From Tab. 5, “+STAM” receives a better VMAF score and perceptual measurements than the baseline. Meanwhile, SDATC overcomes other generation methods in VMAF. The STAM module benefits the spatio-temporal performance of the diffusion model. We also demonstrate temporal profiles in Fig. 7 to compare temporal consistency, SDATC achieves smoother multi-frame reconstruction and is closer to GT frames.

6 Conclusion

In this paper, we presented a Spatial Degradation-Aware and Temporal Consistent (SDATC) diffusion model for compressed video super-resolution. The key of SDATC was leveraging pre-trained diffusion model generation priors and extracting compression priors to improve reconstruction. Specifically, we introduced a distortion control module to modulate diffusion inputs and create controllable guidance, which alleviated negative compression impacts in the following denoising process. To further recover compression-lost details, we inserted prompt-based compression-aware modules in latent and reconstruction space to provide prompts for generation. Finally, we proposed a spatio-temporal attention module and optical flow warping to lighten flickering. Extensive experimental evaluations and visual results on benchmark datasets demonstrated the superiority of SDATC over other state-of-the-art methods. Through compression-specific optimizations, we exploited the potentials of the diffusion model in compressed video super-resolution.

References

- [Blog, 2016] NT Blog. Toward a practical perceptual video quality metric, 2016.
- [Chan *et al.*, 2022a] Kelvin CK Chan, Shangchen Zhou, Xiangyu Xu, and Chen Change Loy. BasicVSR++: Improving video super-resolution with enhanced propagation and alignment. In *Proceedings of the IEEE/CVF conference on computer vision and pattern recognition*, pages 5972–5981, 2022.
- [Chan *et al.*, 2022b] Kelvin CK Chan, Shangchen Zhou, Xiangyu Xu, and Chen Change Loy. Investigating tradeoffs in real-world video super-resolution. In *Proceedings of the IEEE/CVF Conference on Computer Vision and Pattern Recognition*, pages 5962–5971, 2022.
- [Chen *et al.*, 2024] Zhikai Chen, Fuchen Long, Zhaofan Qiu, Ting Yao, Wengang Zhou, Jiebo Luo, and Tao Mei. Learning spatial adaptation and temporal coherence in diffusion models for video super-resolution. In *Proceedings of the IEEE/CVF Conference on Computer Vision and Pattern Recognition*, pages 9232–9241, 2024.
- [Dai *et al.*, 2017] Jifeng Dai, Haozhi Qi, Yuwen Xiong, Yi Li, Guodong Zhang, Han Hu, and Yichen Wei. Deformable convolutional networks. In *Proceedings of the IEEE international conference on computer vision*, pages 764–773, 2017.
- [Ding *et al.*, 2020] Keyan Ding, Kede Ma, Shiqi Wang, and Eero P Simoncelli. Image quality assessment: Unifying structure and texture similarity. *IEEE transactions on pattern analysis and machine intelligence*, 44(5):2567–2581, 2020.
- [Heusel *et al.*, 2017] Martin Heusel, Hubert Ramsauer, Thomas Unterthiner, Bernhard Nessler, and Sepp Hochreiter. Gans trained by a two time-scale update rule converge to a local nash equilibrium. *Advances in neural information processing systems*, 30, 2017.
- [Jo *et al.*, 2018] Younhyun Jo, Seoung Wug Oh, Jaeyeon Kang, and Seon Joo Kim. Deep video super-resolution network using dynamic upsampling filters without explicit motion compensation. In *Proceedings of the IEEE conference on computer vision and pattern recognition*, pages 3224–3232, 2018.
- [Kappeler *et al.*, 2016] Armin Kappeler, Seunghwan Yoo, Qiqin Dai, and Aggelos K Katsaggelos. Video super-resolution with convolutional neural networks. *IEEE transactions on computational imaging*, 2(2):109–122, 2016.
- [Kingma, 2014] DP Kingma. Adam: a method for stochastic optimization. *arXiv preprint arXiv:1412.6980*, 2014.
- [Li *et al.*, 2021] Yinxiao Li, Pengchong Jin, Feng Yang, Ce Liu, Ming-Hsuan Yang, and Peyman Milanfar. Comisr: Compression-informed video super-resolution. In *Proceedings of the IEEE/CVF international conference on computer vision*, pages 2543–2552, 2021.
- [Liang *et al.*, 2021] Jingyun Liang, Jiezhang Cao, Guolei Sun, Kai Zhang, Luc Van Gool, and Radu Timofte. Swinir: Image restoration using swin transformer. In *Proceedings of the IEEE/CVF international conference on computer vision*, pages 1833–1844, 2021.
- [Liang *et al.*, 2022] Jie Liang, Hui Zeng, and Lei Zhang. Details or artifacts: A locally discriminative learning approach to realistic image super-resolution. In *Proceedings of the IEEE/CVF Conference on Computer Vision and Pattern Recognition*, pages 5657–5666, 2022.
- [Liang *et al.*, 2024] Jingyun Liang, Jiezhang Cao, Yuchen Fan, Kai Zhang, Rakesh Ranjan, Yawei Li, Radu Timofte, and Luc Van Gool. Vrt: A video restoration transformer. *IEEE Transactions on Image Processing*, 2024.
- [Lin *et al.*, 2025] Xinqi Lin, Jingwen He, Ziyang Chen, Zhaoyang Lyu, Bo Dai, Fanghua Yu, Yu Qiao, Wanli Ouyang, and Chao Dong. Diffbir: Toward blind image restoration with generative diffusion prior. In *European Conference on Computer Vision*, pages 430–448. Springer, 2025.
- [Liu and Sun, 2013] Ce Liu and Deqing Sun. On bayesian adaptive video super resolution. *IEEE transactions on pattern analysis and machine intelligence*, 36(2):346–360, 2013.
- [Mittal *et al.*, 2012] Anish Mittal, Rajiv Soundararajan, and Alan C Bovik. Making a “completely blind” image quality analyzer. *IEEE Signal processing letters*, 20(3):209–212, 2012.
- [Nah *et al.*, 2019] Seungjun Nah, Sungyong Baik, Seokil Hong, Gyeongsik Moon, Sanghyun Son, Radu Timofte, and Kyoung Mu Lee. Ntire 2019 challenge on video deblurring and super-resolution: Dataset and study. In *Proceedings of the IEEE/CVF conference on computer vision and pattern recognition workshops*, pages 0–0, 2019.
- [Potlapalli *et al.*, 2024] Vaishnav Potlapalli, Syed Waqas Zamir, Salman H Khan, and Fahad Shahbaz Khan. Promptir: Prompting for all-in-one image restoration. *Advances in Neural Information Processing Systems*, 36, 2024.
- [Qiu *et al.*, 2022] Zhongwei Qiu, Huan Yang, Jianlong Fu, and Dongmei Fu. Learning spatiotemporal frequency-transformer for compressed video super-resolution. In *European Conference on Computer Vision*, pages 257–273. Springer, 2022.
- [Rombach *et al.*, 2022] Robin Rombach, Andreas Blattmann, Dominik Lorenz, Patrick Esser, and Björn Ommer. High-resolution image synthesis with latent diffusion models. In *Proceedings of the IEEE/CVF conference on computer vision and pattern recognition*, pages 10684–10695, 2022.
- [Saharia *et al.*, 2022] Chitwan Saharia, Jonathan Ho, William Chan, Tim Salimans, David J Fleet, and Mohammad Norouzi. Image super-resolution via iterative refinement. *IEEE transactions on pattern analysis and machine intelligence*, 45(4):4713–4726, 2022.
- [Sun *et al.*, 2023] Lingchen Sun, Rongyuan Wu, Zhengqiang Zhang, Hongwei Yong, and Lei Zhang. Improving the stability of diffusion models for content consistent super-resolution. *arXiv preprint arXiv:2401.00877*, 2023.

- [Sun *et al.*, 2024] Haoze Sun, Wenbo Li, Jianzhuang Liu, Haoyu Chen, Renjing Pei, Xueyi Zou, Youliang Yan, and Yujiu Yang. Coser: Bridging image and language for cognitive super-resolution. In *Proceedings of the IEEE/CVF Conference on Computer Vision and Pattern Recognition*, pages 25868–25878, 2024.
- [Tian *et al.*, 2020] Yapeng Tian, Yulun Zhang, Yun Fu, and Chenliang Xu. TDAN: Temporally-deformable alignment network for video super-resolution. In *Proceedings of the IEEE/CVF conference on computer vision and pattern recognition*, pages 3360–3369, 2020.
- [Wang *et al.*, 2019] Xintao Wang, Kelvin CK Chan, Ke Yu, Chao Dong, and Chen Change Loy. EDVR: Video restoration with enhanced deformable convolutional networks. In *Proceedings of the IEEE/CVF conference on computer vision and pattern recognition workshops*, pages 1954–1963, 2019.
- [Wang *et al.*, 2021] Xintao Wang, Liangbin Xie, Chao Dong, and Ying Shan. Real-esrgan: Training real-world blind super-resolution with pure synthetic data. In *Proceedings of the IEEE/CVF international conference on computer vision*, pages 1905–1914, 2021.
- [Wang *et al.*, 2023a] Jianyi Wang, Kelvin CK Chan, and Chen Change Loy. Exploring clip for assessing the look and feel of images. In *Proceedings of the AAAI Conference on Artificial Intelligence*, volume 37, pages 2555–2563, 2023.
- [Wang *et al.*, 2023b] Yingwei Wang, Takashi Isobe, Xu Jia, Xin Tao, Huchuan Lu, and Yu-Wing Tai. Compression-aware video super-resolution. In *Proceedings of the IEEE/CVF Conference on Computer Vision and Pattern Recognition*, pages 2012–2021, 2023.
- [Wang *et al.*, 2024] Jianyi Wang, Zongsheng Yue, Shangchen Zhou, Kelvin CK Chan, and Chen Change Loy. Exploiting diffusion prior for real-world image super-resolution. *International Journal of Computer Vision*, pages 1–21, 2024.
- [Wiegand *et al.*, 2003] Thomas Wiegand, Gary J Sullivan, Gisle Bjontegaard, and Ajay Luthra. Overview of the h. 264/avc video coding standard. *IEEE Transactions on circuits and systems for video technology*, 13(7):560–576, 2003.
- [Wu *et al.*, 2024] Rongyuan Wu, Tao Yang, Lingchen Sun, Zhengqiang Zhang, Shuai Li, and Lei Zhang. Seesr: Towards semantics-aware real-world image super-resolution. In *Proceedings of the IEEE/CVF conference on computer vision and pattern recognition*, pages 25456–25467, 2024.
- [Yang *et al.*, 2021] Xi Yang, Wangmeng Xiang, Hui Zeng, and Lei Zhang. Real-world video super-resolution: A benchmark dataset and a decomposition based learning scheme. In *Proceedings of the IEEE/CVF International Conference on Computer Vision*, pages 4781–4790, 2021.
- [Yang *et al.*, 2022] Sidi Yang, Tianhe Wu, Shuwei Shi, Shanshan Lao, Yuan Gong, Mingdeng Cao, Jiahao Wang, and Yujiu Yang. Maniqa: Multi-dimension attention network for no-reference image quality assessment. In *Proceedings of the IEEE/CVF Conference on Computer Vision and Pattern Recognition*, pages 1191–1200, 2022.
- [Yang *et al.*, 2025] Xi Yang, Chenhang He, Jianqi Ma, and Lei Zhang. Motion-guided latent diffusion for temporally consistent real-world video super-resolution. In *European Conference on Computer Vision*, pages 224–242. Springer, 2025.
- [Yu *et al.*, 2019] Peng Yi, Zhongyuan Wang, Kui Jiang, Junjun Jiang, and Jiayi Ma. Progressive fusion video super-resolution network via exploiting non-local spatio-temporal correlations. In *Proceedings of the IEEE/CVF international conference on computer vision*, pages 3106–3115, 2019.
- [Yu *et al.*, 2024] Fanghua Yu, Jinjin Gu, Zheyuan Li, Jinfan Hu, Xiangtao Kong, Xintao Wang, Jingwen He, Yu Qiao, and Chao Dong. Scaling up to excellence: Practicing model scaling for photo-realistic image restoration in the wild. In *Proceedings of the IEEE/CVF Conference on Computer Vision and Pattern Recognition*, pages 25669–25680, 2024.
- [Zhang *et al.*, 2023] Lvmin Zhang, Anyi Rao, and Maneesh Agrawala. Adding conditional control to text-to-image diffusion models. In *Proceedings of the IEEE/CVF International Conference on Computer Vision*, pages 3836–3847, 2023.
- [Zhou *et al.*, 2024] Shangchen Zhou, Peiqing Yang, Jianyi Wang, Yihang Luo, and Chen Change Loy. Upscale-a-video: Temporal-consistent diffusion model for real-world video super-resolution. In *Proceedings of the IEEE/CVF Conference on Computer Vision and Pattern Recognition*, pages 2535–2545, 2024.

7 Appendix

Due to the lack of space in the main paper, we provide more details of the proposed Spatial Degradation-Aware and Temporal Consistent (SDATC) diffusion model in supplementary material. In Appendix 1.1, we present more information on the baseline LDM diffusion model. Additional experimental results and visual comparisons can be found in Appendix 1.2.

7.1 Methodology

This section supplements the section “Methodology” in the main paper. We present a detailed introduction to our SDATC’s benchmark framework.

Color Correction

Recent works [Choi et al. 2022] have found that diffusion models confront color shift issues. Noting that the variant network of diffusion models exhibits a more noticeable color shift issue after training, Upscale-A-Video [Zhou et al., 2024] adopted the wavelet color correction module [Wang et al., 2024] for correction. Specifically, Upscale-A-Video performed color normalization on generated images by referencing the mean and variance of LR inputs. Carrying on the same line of thought, we adopt adaptive instance normalization (adaIN) [Huang and Belongie 2017] to transform the style of reconstructed frames to have similar color and illuminations as those LQ frames in SDATC.

7.2 Experiments

In this section, we provide more quantitative and qualitative experimental results to compare the proposed SDATC with other state-of-the-art methods comprehensively. We also supply additional ablation study results to claim the effectiveness of the proposed modules.

Quantitative Comparison

As can be seen from Tab. 1, we introduce additional experiments on the Vid4 dataset. We also follow the compression level setting in the main paper, CRF=15, 25, and 35 for $\times 4$ VSR. SDATC outperforms other methods in terms of perceptual quality, especially in MANIQA [Yang et al., 2022] and CLIP-IQA [Wang et al., 2023a], which highly correlate with human perception. Similar to other diffusion-based methods, the proposed STDAC shows limitations on certain metrics like PSNR and SSIM because these metrics are primarily designed to measure pixel-level fidelity and structural similarity, while STDAC focuses on perceptual quality. Notably, our STDAC performs better than SOTA diffusion-based SISR approach StaleSR and VSR approach MGLD-VSR on PSNR and SSIM. The comprehensive experimental results deflect the great capability of SDATC to enhance compressed videos and carry out realistic details.

Qualitative Comparison

We visualize $\times 4$ VSR qualitative results in Fig. 3, Fig. 4, and Fig. 5. As can be seen in zoom-in regions, SDATC reconstructs more appealing structure textures and more complete buildings. For MSE-based methods, their reconstruction results are totally blurred, especially when CRF is 25 or 35. Although other generation models could recover objects from compressed frames, a sense of unreality from their

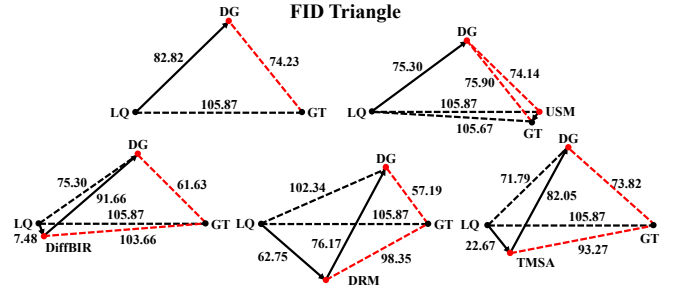


Figure 9: FID scores of different restoration methods.

SDATC (Ours)	71%	RealBasicVSR
SDATC (Ours)	76%	StableSR
SDATC (Ours)	60%	MGLD-VSR

Figure 10: Visual results of different restoration methods.

reconstruction results has a negative impact on visual experiences. Benefiting from the strong generation priors, SDATC develops finer details and less compression artifacts.

Ablation of Distortion Control Module

As mentioned in the section “Ablation Study” of the main paper, we illustrate the FID [Heusel et al. 2017] scores of different methods in Fig. 1. It can be observed that DCM achieves the best FID score between the DG domain and GT domain, which means DCM allows the diffusion model to achieve the most similar outputs with GT frames. We also visualize the results of these methods in Fig. 2, DCM effectively deduces noises and provides smooth diffusion inputs.

Table 6: Quantitative comparison of $\times 4$ VSR on different compression levels Vid4 dataset. **Bold** and underlined values denote the best and second-best results respectively. \uparrow and \downarrow indicate better quality with higher and lower values correspondingly.

Dataset		Vid4							
Method	CRF	PSNR \uparrow	SSIM \uparrow	LPIPS \downarrow	DISTS \downarrow	FID \downarrow	NIQE \downarrow	MANIQA \uparrow	CLIP-IQA \uparrow
BasicVSR++	15	<u>25.74</u>	0.7381	0.3745	0.1566	<u>68.73</u>	5.137	0.2155	0.4110
VRT	15	25.72	<u>0.7418</u>	0.3747	0.1680	70.73	5.939	0.2253	0.4202
FTVSR	15	26.35	0.7849	0.3634	0.1439	68.93	5.584	0.2947	0.5597
Real-ESRGAN	15	22.42	0.6037	0.3838	0.1516	86.16	2.593	0.3336	0.5924
RealBasicVSR	15	23.92	0.6615	0.3526	<u>0.1252</u>	72.95	<u>2.933</u>	0.2922	0.6185
StableSR	15	22.15	0.5805	0.3762	0.1430	80.16	3.207	0.3380	<u>0.6460</u>
MGLD-VSR	15	22.27	0.5654	0.3741	0.1321	89.46	3.247	<u>0.3529</u>	0.6292
SDATC (Ours)	15	22.49	0.5862	<u>0.3631</u>	0.1229	65.97	3.055	0.3714	0.7332
BasicVSR++	25	23.64	0.6210	0.4738	0.2183	137.96	5.621	0.1594	0.2703
VRT	25	<u>23.79</u>	<u>0.6300</u>	0.4717	0.2266	137.68	6.532	0.1663	0.3271
FTVSR	25	24.70	0.6980	0.4217	0.1984	131.18	6.106	0.2548	0.4861
Real-ESRGAN	25	21.96	0.5703	0.4206	0.1672	115.83	2.662	0.3175	0.5899
RealBasicVSR	25	22.82	0.5931	0.4163	0.1588	116.50	<u>2.809</u>	0.2712	0.5987
StableSR	25	21.85	0.5561	0.4094	0.1588	<u>93.54</u>	3.416	0.3056	<u>0.6264</u>
MGLD-VSR	25	21.77	0.5290	<u>0.4073</u>	<u>0.1507</u>	97.76	3.276	<u>0.3447</u>	0.6051
SDATC (Ours)	25	21.91	0.5362	0.4055	0.1436	92.56	3.157	0.3666	0.6979
BasicVSR++	35	21.57	0.4914	0.5838	0.2885	254.62	6.618	0.1114	0.1421
VRT	35	<u>21.62</u>	<u>0.4949</u>	0.5844	0.2907	252.83	7.157	0.1228	0.1806
FTVSR	35	22.08	0.5412	0.5497	0.2786	302.37	6.898	0.1813	0.1840
Real-ESRGAN	35	20.83	0.4874	0.5204	0.2304	235.89	3.213	0.2382	0.4272
RealBasicVSR	35	20.98	0.4783	0.5229	0.2229	250.18	<u>3.113</u>	0.2326	0.3449
StableSR	35	20.89	0.4815	0.5186	0.2368	<u>222.96</u>	4.246	0.2102	0.3748
MGLD-VSR	35	20.46	0.4392	<u>0.5023</u>	<u>0.2083</u>	166.07	3.054	<u>0.3234</u>	<u>0.4396</u>
SDATC (Ours)	35	20.27	0.4077	0.4773	0.1919	231.08	3.256	0.3501	0.5994

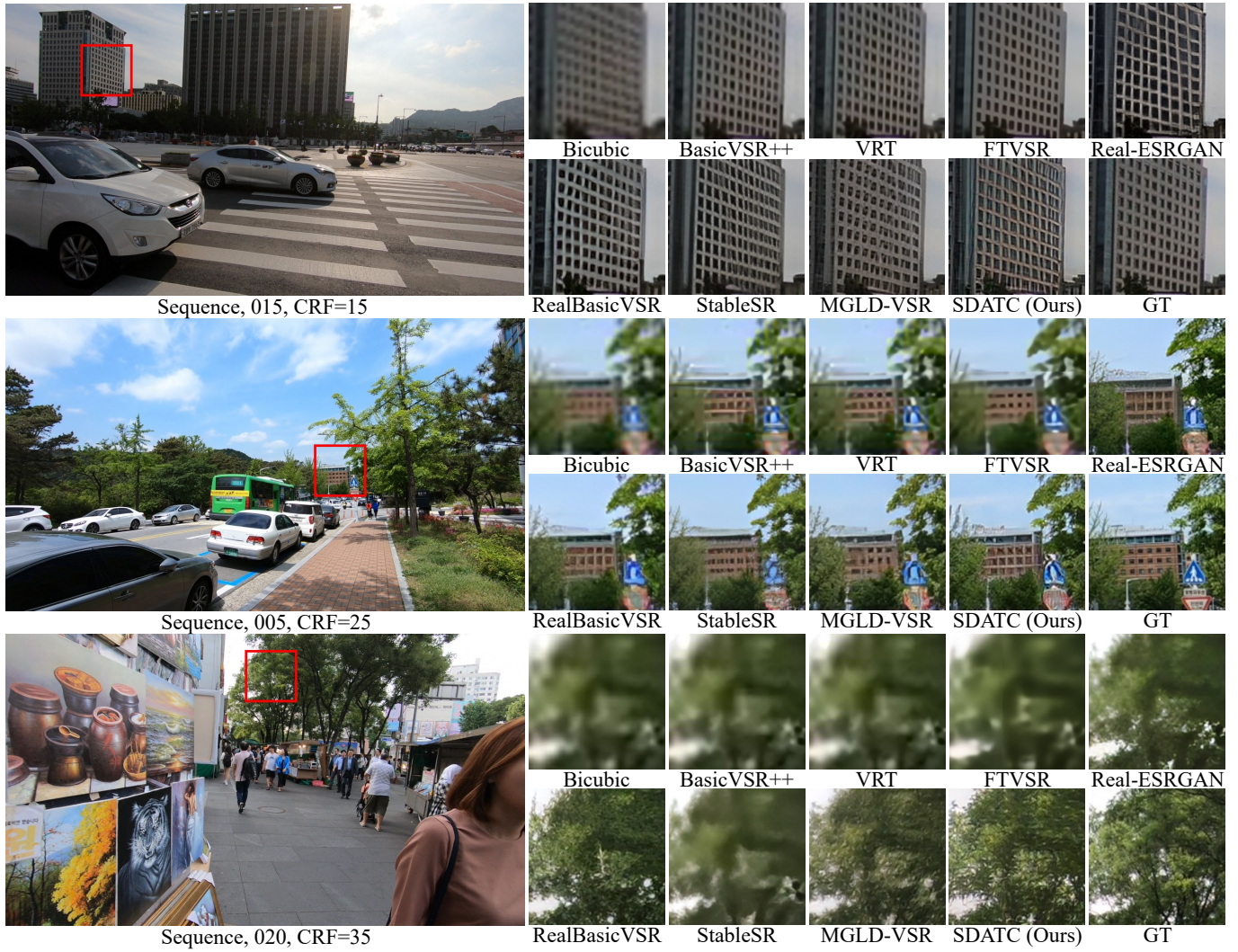


Figure 11: Qualitative comparison of $\times 4$ VSR on different compression level REDS4 dataset.

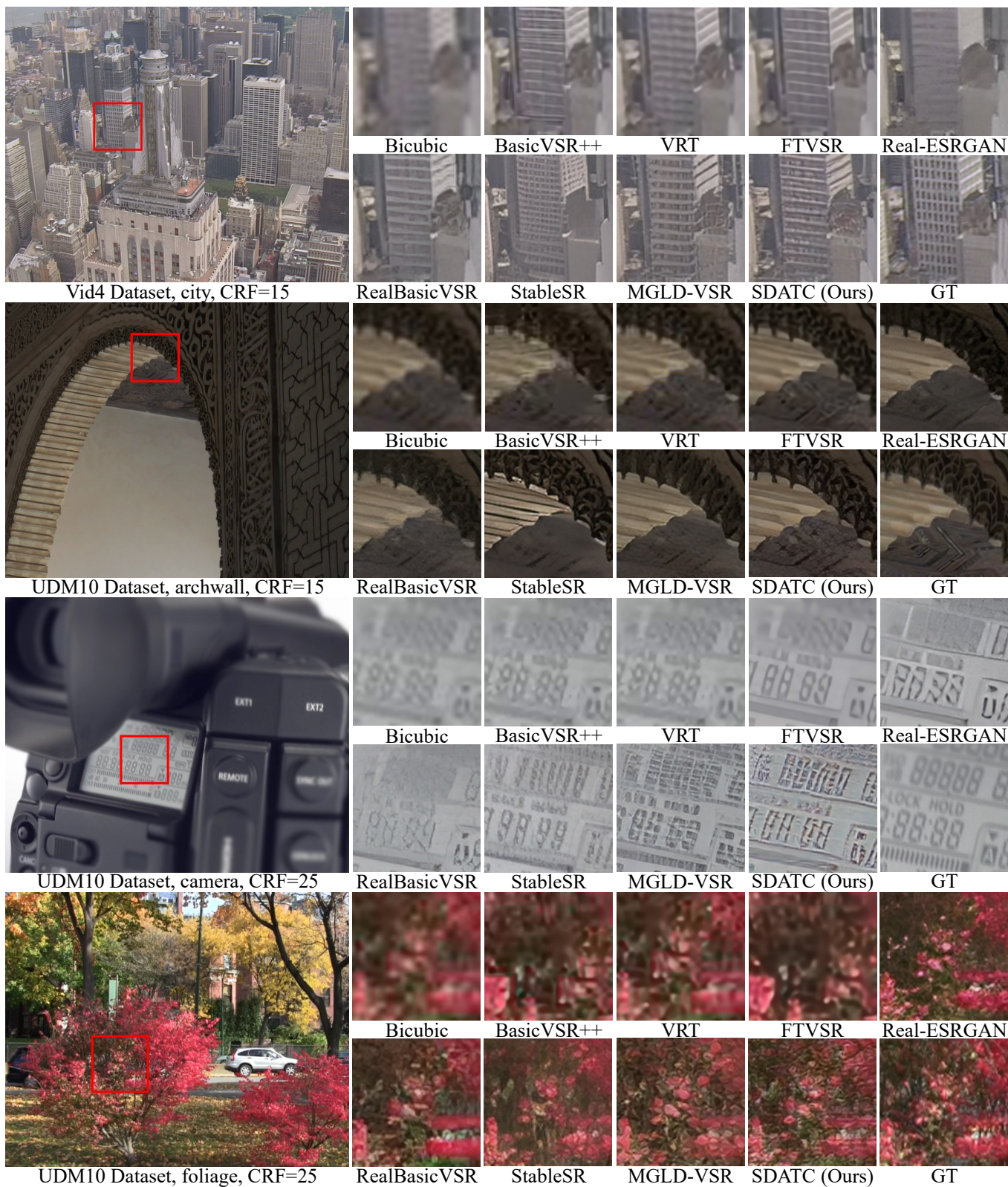


Figure 12: Qualitative comparison of $\times 4$ VSR on different compression level datasets.

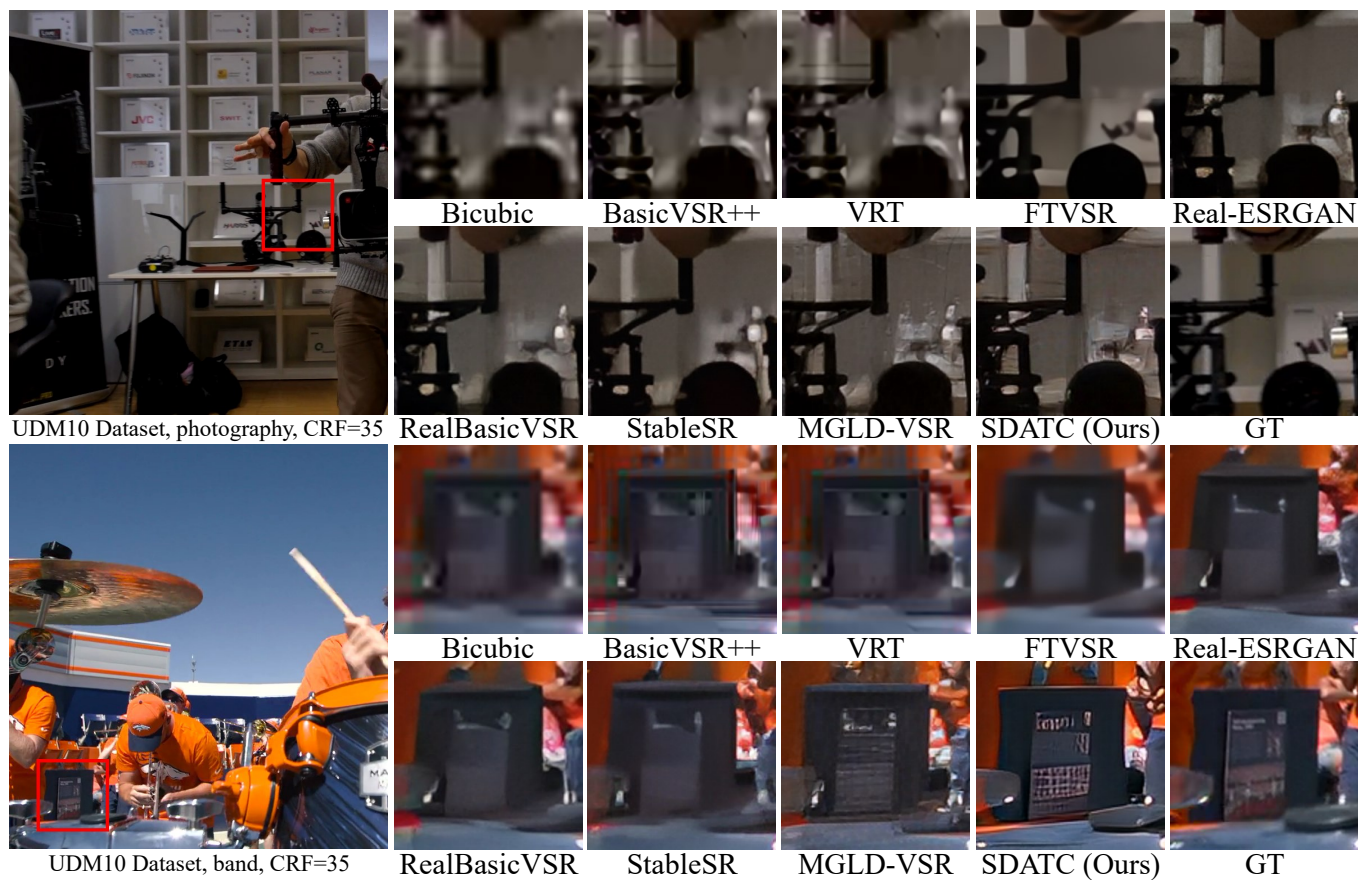


Figure 13: Qualitative comparison of $\times 4$ VSR on different compression level datasets.